Fairness Optimization for VLC Systems With Liquid Crystal-Based RIS-Enabled Transmitters

Xin-Yu Zhang, Jian Zhang, and Qi Wu

***Abstract*—The application of liquid crystal (LC)-based reconfigurable intelligent surface (RIS)-assisted transmitters in visible light communication (VLC) systems can guide and amplify the light emitted by light emitting diodes (LEDs). In this paper, we investigate the VLC system employing the RIS-assisted transmitter, where user fairness is maximized by optimizing the refractive index of the RIS module. To address the non-convex problem, we adopt the particle swarm optimization (PSO) algorithm. Simulation results illustrate that equipping the RIS-assisted transmitter in the system and using the proposed algorithm can significantly improve user fairness.**

***Index Terms*—Liquid crystal, reconfigurable intelligent surface, visible light communication, fairness.**

I. Introduction

THE ever-growing desire for more wireless access capacity has prompted visible light communication (VLC) to become an attractive radio frequency (RF) communications supplementary technology for promoting higher communication rates in the upcoming generation of networks for communication [1]. VLC is regarded as an economical and highly energy-effective implementation since the VLC system utilizes light emitting diodes (LEDs) as transmitters. In addition to the energy-saving property, VLC presents further outstanding advantages compared with RF communications, such as high security in indoor environments (where optical rays can not penetrate the walls) or the ability to perform illumination and communication simultaneously [2]. Although VLC technology has numerous advantages, limitations such as line-of-sight (LoS) blockages [3], random device orientation [4], and inadequate user fairness hinder its advancement in the future.

Reconfigurable intelligent surface (RIS) has gained significant interest in RF communication systems for its ability to reconfigure wireless propagation proactively [5]. In recent years, research on the application of RIS technology in VLC networks has risen. Specifically, inserting the RIS into the VLC system can enhance the received signal power, expand communication and illumination coverage [6], and improve the VLC capacity [7]. Implementing RIS in the VLC system is based on principles such as reflection and refraction of optics to modify the optical signal and enhance VLC performance [5]. For instance, mirror array-based RIS technology utilizes the reflection of optics to alleviate the problem of blockages in the indoor environment [4]. Additionally, liquid crystal (LC)-based RIS exploits its refractive characteristics to adjust incident light in receivers dynamically.

Most previous efforts have been dedicated to studying using RIS in the channel to improve VLC communication performance [4], [8]. Several studies have investigated the channel model for VLC systems utilizing the LC RIS-enabled receiver in [3], [9], [10]. To jointly benefit from optical RISs, authors in [11] proposed that the optical simultaneous transmission and reflection reconfigurable intelligent surface (OSTAR-RIS) consists of mirror array-based RIS elements as reflectors and LC RIS elements as refractors to steer and amplify the signals to enhance the VLC system communication performance gain. Moreover, the RIS can be employed in the transmitter as a refractive element to enhance beam strength and orientation. However, the former literature barely investigated deploying the RIS at the transmitter side to achieve performance improvements. The work in [5] proposed that the LC RIS is an appropriate technology to install at the front end of the transmitter because of its adjustable refractive index. Integrating the LC RIS into the transmitter can focus, steer, and amplify the transmitted light with the help of the RIS controller to achieve some system performance improvements, such as communication and illumination coverage extension and dynamic beam directivity enhancement. In [6], the authors applied a fixed parameter of the RIS element to study RIS-enabled transmitters with various LED array layouts for improving lighting and communication coverage.

Regarding optimizing RIS configuration, research interests mainly focus on optimizing achievable data rates [3], [4], channel capacity [7], and spectrum efficiency. The design of these optimization problems neglected to account for changes in channel strength resulting from the user's location. When the channel strength anywhere on the receiving plane in the communication system varies notably, poor user communication performance will be severely impacted, thus affecting the quality of service [6]. As such, fairness is required to be considered as an indicator of performance while designing optimization problems. The authors in [12] presented optimization problems for maximizing sum rate and fairness by controlling the specular reflecting RIS and diffuse reflecting RIS in the channel. Note that although the work in [12] optimized user fairness, it only considered a few users' presence and employed reflecting RISs

Manuscript received 9 July 2024; accepted 11 July 2024. Date of publication 16 July 2024; date of current version 23 July 2024. This work was supported by the National Natural Science Foundation of China (NSFC) under Grant 62071489. *(Corresponding author: Jian Zhang.)*

The authors are with the National Digital Switching System Engineering and Technological Research Center, Zhengzhou 450000, China (e-mail: xiaoxin_05061@126.com; Zhang_xinda@126.com; qi_wu5757@163.com).

Digital Object Identifier 10.1109/JPHOT.2024.3429187

in the VLC system. Moreover, the authors in [6] evaluated the improvement effect of RIS-enabled transmitters on uniformity. However, this work employed a fixed parameter of LC, and uniformity is defined as the ratio between the minimum rate received by the user on the receiving plane and the average rate.

In this paper, we propose optimizing the RIS element's refractive index to improve the communication performance for the users on the receiving plane in an indoor VLC system by maximizing fairness. We adopt a fairness index (FI) to assess the fairness of users [13], [14]. Due to the non-convexity of the proposed optimization problem, we adopt the particle swarm optimization (PSO) algorithm, which has been used to tackle the optimization problems in the RIS-assisted VLC fields [12], to solve it. The main contributions of our work can be summarized as follows:

- We explore an indoor VLC system where the RIS module is deployed at the transmitter end, and the effect of wall reflective paths is considered.
- We propose the refractive index of the RIS element optimization problem to improve user fairness. Since the formulated problem is non-convex, we use the PSO algorithm to solve it.
- Further, we illustrate the proposed algorithm's effectiveness. We additionally evaluate the extent of enhancement in LoS and NLoS links for the poorest user by positioning the LC RIS at the transmitter end.
- Finally, we analyze in detail how the channel gain for NLoS links is affected by different practical parameters like the height of wall sub-regions from the floor and wall reflection coefficient.

The rest of this article is structured as follows. In Section II, we describe the constructional detail of the transmitter and the VLC system model assisted by an LC-based RIS-enabled transmitter. Next, we formulate the optimization problem mathematically and adopt a PSO algorithm to solve it in Section III. Finally, we discuss the simulation results in Section IV and make conclusions in Section V.

II. System Model

This section presents a layout of the indoor environment, a description of the configuration of the RIS-enabled transmitter, and its ability to manipulate light emission from the LED. Then, the channel models for the directed link and non-directed paths are presented, and finally, the total channel gain of the system model is provided.

A. Indoor VLC System Description

An indoor VLC system comprises an LED lamp with a nematic LC RIS, the channel, and receivers, each equipped with a photodiode (PD), as shown in the left part of Fig. 1. The transmitter takes advantage of LC RIS technology, positioning it at the front of the LED lamp, which differs from ordinary VLC transmitters. Specifically, an LC-based RIS typically consists of some layers such as polarizers, glass substrate, indium tin oxide (ITO) films, and photoalignment layer. The polarizer filters any light emitted from the LED array except for wavelengths

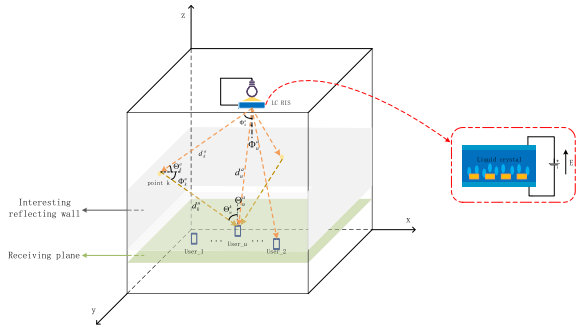

Fig. 1. Illustrations of the proposed system with the LC-based RIS-enabled transmitter.

containing the conveyed signals [5]. The glass substrates exhibit a preferential orientation. Additionally, the ITO material helps generate and control heat.

The light signal travels through the RIS module once an external electric field value exceeds the threshold voltage. More specifically, the light signal emitted by the LED impinges on the top interface between two mediums of air and LC with different refractive indices. Some of it is reflected at the top interface of the LC cell, while the rest is refracted because there is no phenomenon of light absorption on the surface. The right part of the Fig. 1 illustrates how an external voltage can influence the re-orientation of molecules in the LC cell, allowing control over the propagation characteristics of the light signal, such as orientation and intensity. Applying a variable external electric field induces the LC molecules to reorient their original direction to become perpendicular to the glass. Note that the re-orientation of molecule responses can be characterized by the refractive index of the RIS. Therefore, the refractive index is the primary factor affecting the variation in wave-guiding capabilities.

B. LC-Based RIS-Enabled Transmitter: Lighting Steering and Optical Amplification

This subsection describes how the orientation and intensity of a light beam change as it moves through the RIS module. The result of the RIS element on the overall channel gain can be characterized by the transition coefficient in VLC systems. Moreover, the transition coefficient can be acquired by analyzing the light propagation process, which includes the emission of light from the LED traveling through the air to the LC cell and ultimately through the LC cell back to the air. The angular reflectance refers to the proportion of incident light reflected at the top layer of an LC cell when the incident light is unpolarized [15]. The reflection of light when the light signal impinges at the top interface of the RIS can be quantified as [3]:

$$R_{ac}(\Phi_k^a) = \frac{1}{2}\left(\frac{\eta^2\cos(\Phi_k^a) - \sqrt{\eta^2 - \sin^2(\Phi_k^a)}}{\eta^2\cos(\Phi_k^a) + \sqrt{\eta^2 - \sin^2(\Phi_k^a)}}\right)^2 + \frac{1}{2}\left(\frac{\cos(\Phi_k^a) - \sqrt{\eta^2 - \sin^2(\Phi_k^a)}}{\cos(\Phi_k^a) + \sqrt{\eta^2 - \sin^2(\Phi_k^a)}}\right)^2, \quad (1)$$

where $\eta = \eta_c/\eta_a$ denotes the relative refractive index when the light enters the LC cell, Φ_k^a is the angle of incidence at the top interface of the RIS, η_c and η_a represent the refractive indices of the liquid crystal and air medium, respectively. When the light emerges from the LC element, the angular reflectance can be calculated by:

$$R_{ca}(\zeta) = \frac{1}{2}\left(\frac{\eta_1^2\cos(\zeta) - \sqrt{\eta_1^2 - \sin^2(\zeta)}}{\eta_1^2\cos(\zeta) + \sqrt{\eta_1^2 - \sin^2(\zeta)}}\right)^2 + \frac{1}{2}\left(\frac{\cos(\zeta) - \sqrt{\eta_1^2 - \sin^2(\zeta)}}{\cos(\zeta) + \sqrt{\eta_1^2 - \sin^2(\zeta)}}\right)^2, \quad (2)$$

where $\eta_1 = \eta_a/\eta_c$ denotes the relative refractive index when the light signal emits from the LC cell, $\zeta = \arcsin(\eta_a\Phi_k^a/\eta_c)$ is the angle of refraction defined by Snell's law and indicates the light orientation in the LC module. Regarding how much of the light is refracted, because all of the light is refracted at the interface without any absorption when the light signal comes from the air and LC-based RIS, the angular transmittance is given as follows:

$$T_{ac}(\Phi_k^a) = (1 - R_{ac}(\Phi_k^a)), \quad (3)$$

$$T_{ca}(\zeta) = (1 - R_{ca}(\zeta)). \quad (4)$$

Then, the transition coefficient of the NLoS path can be expressed as [3]:

$$\alpha_{\text{LC}-\text{NLoS}} = T_{ac}(\Phi_k^a)T_{ca}(\zeta). \quad (5)$$

When considering the LoS path, the transition coefficient $\alpha_{\text{LC}-\text{LoS}}$ is similarly expressed as $\alpha_{\text{LC}-\text{NLoS}}$ with Φ_k^a, ζ replaced by Φ_u^a, ζ', respectively:

$$\alpha_{\text{LC}-\text{LoS}} = T_{ac}(\Phi_u^a)T_{ca}(\zeta'). \quad (6)$$

Finally, we can deduce from (1) to (6) that the refractive index can control the transition coefficient. In addition, the tilt angle δ can be used to specify the orientation of molecules within the LC cell, the η_c can be expressed as a function of the tilt angle δ [16]:

$$\frac{1}{\eta_c^2(\delta)} = \frac{\cos^2(\delta)}{\eta_e^2} + \frac{\sin^2(\delta)}{\eta_o^2}, \quad (7)$$

where $\eta_c(\delta)$ represents the refractive index at a specific tilt angle, η_o and η_e denote the ordinary and extraordinary refractive indices, respectively. The effect of an externally controlled voltage on the tilt angle can be specified by [17]:

$$\delta = \begin{cases} \frac{\pi}{2} - 2\tan^{-1}[\exp(-\frac{v_e - v_{th}}{v_0})], & v_e > v_{th} \\ 0, & \text{otherwise} \end{cases} \quad (8)$$

where v_e represents an external voltage, v_{th} represents the threshold voltage indicating that the LC molecules begin to tilt, and v_0 is a fixed value. Therefore, we can consider that the LC element is the RIS for voltage control, capable of directing the light rays.

Next, we introduce the amplification gain. The amplification gain is a crucial element for characterizing the amplification light. When the emerging light gains great intensity by an external voltage, this creates an optical amplification. Specifically, the optical intensity emitted from the RIS element exceeds that of the incident light. Further, light amplification occurs by the stimulated emission mechanism, in which a change in atomic population causes the absorption coefficient sign to invert [17]. In LC-based RIS-enabled transmitters, excited by the field, the LC cell creates new coherent photons that move in the same direction as the incident ones. An exponential emission of the emitted light power P' from the LC element can be expressed as follows [10]:

$$P' = P \times \exp(\Gamma d) \times \alpha_{\text{LC}}, \quad (9)$$

where d denotes the thickness of the LC RIS, and P is the optical power. Based on the dynamic coupling theory, the gain coefficient Γ in (9) can be given by [3]:

$$\Gamma = \frac{2\pi\eta_c^3}{\lambda\cos(\Phi)} r_{\text{eff}} E, \quad (10)$$

where λ is the wavelength of the incident light, r_{eff} represents the electro-optic coefficient, and E represents the strength of the charge field calculated by [*V*/m], which means the applied voltage divided by the thickness of LC RIS. Therefore, the amplification gain coefficient mainly depends on the refractive index, wavelength, incident angle, and externally applied voltage. Consequently, we consider the refractive index as a decision variable in our optimization problem for improving communication performance.

C. VLC Channel

This work considers that the overall channel gain can be categorized as the LoS link between the communication devices and non-LoS links relying on the wall reflections. Due to the deployment of the RIS at the transmitting end, we consider the channel gain of directed and non-directed links as a combination of two parts.

The first part involves how light propagates through the RIS, modifying the properties of the incident light. The propagation process in the first part can be characterized as [3]:

$$\varepsilon = \alpha_{\text{LC}} \times \exp(\Gamma d). \quad (11)$$

The second component is as a result of the emitted light traveling through the air to the receiver. As mentioned in [18], both directed and non-directed channels can be modeled as the Lambertian radiation model. The channel gain of the LoS link for the u-th user can be represented as [19]:

$$H_{\text{LoS}}^u = \begin{cases} \frac{(m+1)A_{\text{PD}}}{2\pi(d_u^a)^2}\cos^m(\Phi_u^a)T(\Theta_u^a)G(\Theta_u^a)\cos(\Theta_u^a), & 0 \le \Theta_u^a \le \Theta_{\text{FoV}} \\ 0, & \Theta_u^a > \Theta_{\text{FoV}} \end{cases} \quad (12)$$

where $m = -1/log_2(\cos(\Phi_{1/2}))$ denotes the Lambertian index with $\Phi_{1/2}$ as the semi-angle of the FoV of the LED, A_{PD} represents the area of PD, and d_u^a is the distance of the directed path between the LED and the u-th PD. Then, Φ_u^a represents the angle of irradiance at the LED, Θ_u^a is the angle of incidence at the u-th PD, Θ_{FoV} is the PD's FoV, $T(\Theta_u^a)$ represents the gain

of the optical filter, and the gain of the optical concentrator is given as $G(\Theta_u^a) = f^2/\sin^2(\Theta_{\text{FoV}})$ with f as the refractive index of the concentrator.

The NLoS channel is composed of two parts. A reflective element is regarded as a receiver obtaining signals from the novel transmitter and serves as a point source that can re-transmit signals. The wall is divided into K grid reflectors. Since high-order reflections do not significantly impact the VLC system [10], we only consider the first-order reflection from the k-th wall sub-region. We assume that the light from the transmitter hits the center of each reflection element. The channel gain for the NLoS component from the k-th wall surface to the u-th PD is expressed by [19]:

$$H_{u-\text{NLoS}}^k = \begin{cases} \rho_{\text{wall}} \frac{(m+1)A_{\text{PD}}}{2\pi^2 (d_k^a)^2 (d_k^u)^2} dA_k \cos^m(\Phi_k^a)\cos(\Phi_k^u)\cos(\Theta_u^k) \\ \times T(\Theta_k^a) G(\Theta_k^a)\cos(\Theta_k^a), 0 \le \Theta_u^k \le \Theta_{\text{FoV}} \\ 0, \Theta_u^k > \Theta_{\text{FoV}} \end{cases} \tag{13}$$

where the area of each grid is dA_k, ρ_{wall} represents the reflectivity of the wall, d_k^a and d_k^u are the distance from the access point (AP) to the k-th wall reflecting element, and the distance from the reflective surface k to the u-th PD, respectively. Then, Φ_k^a represents the angle of the irradiance for the non-LoS path from the AP to the reflective surface k, and Θ_k^a represents the incidence angle at the k-th reflecting surface. Accordingly, Φ_k^u is the angle of irradiance from the k-th grid to the u-th PD, and Θ_u^k is the incidence angle at the u-th PD.

Finally, we can express the total channel gain of the overall process for the u-th user as follows:

$$H_u = \varepsilon_{\text{LoS}}^u H_{\text{LoS}}^u + \sum_{k=1}^{K} \varepsilon_{u-\text{NLoS}}^k H_{u-\text{NLoS}}^k. \tag{14}$$

III. User Fairness Optimization

A. Fairness Maximization Problem Formulation

To enhance the fairness of user communication and system performance, we propose a user fairness optimization problem. We establish the achievable rate defined in [6] for any user on the receiving plane in an indoor environment served by a system equipped with the LC RIS-assisted transmitter. As a result, in the VLC system supported by the LC RIS-assisted transmitter, the rate for the u-th user can obtain is given as:

$$R_u = Blog_2 \left\{ 1 + \frac{\exp(1)}{2\pi} \times \frac{\left(\frac{P}{q} R_{\text{PD}} \left(\varepsilon_{\text{LoS}}^u H_{\text{LoS}}^u + \sum_{k=1}^{K} \varepsilon_{u-\text{NLoS}}^k H_{u-\text{NLoS}}^k\right)\right)^2}{N_o B} \right\}, \tag{15}$$

where B denotes the system's bandwidth, P is the optical power, q is the ratio of the transmit optical power to the electrical power, N_o indicates the power spectral density of the noise, and R_{PD} represents the optical-electric responsivity coefficient of the PD.

To assess the fairness of user communication, we utilize the FI defined in [13]. It can be stated as a function of the user rate to quantify the fairness of communication between users, which is described as follows:

$$\text{FI} = \frac{1}{N_u} \times \frac{\left(\sum_{u=1}^{N_u} R_u\right)^2}{\sum_{u=1}^{N_u} R_u^2}, \tag{16}$$

where N_u represents the number of users. In addition, FI is bounded between 0 and 1, with FI = 1 representing the best fairness. Thus, the fairness optimization problem can be expressed as:

$$\max_{\eta_c} \ \text{FI}$$
$$\text{s.t.}$$
$$C_1: \ \eta_b \le \eta_c \le \eta_t, \tag{17}$$

where the constraint in (17) η_b and η_t denote the lower and top bound of a typical LC refractive index [20]. The problem is non-convex, and it is challenging to solve. Accordingly, we introduce the PSO algorithm, which has been used to solve optimization problems in VLC systems [12]. The PSO has many advantages, such as quick convergence, few parameter settings, and ease of implementation. We will present the PSO method in detail in the next subsection.

B. Proposed Solution

The pseudocode is shown in Algorithm 1. PSO is one of the popular algorithms in intelligent optimization methods. PSO algorithm is utilized to determine the minimum value or maximum value of a process. This algorithm can be implemented in three basic steps. Initially, the algorithm is initialized, and a set of random particles is generated randomly. Subsequently, the local best and globally optimal solutions are calculated and updated while the particle's direction, velocity, and position are varied during each iteration. Finally, the final optimal result is obtained [12]. This work uses this optimization process to find the optimal refractive index. The proposed PSO algorithm steps are given below in detail.

Assuming the initial population is composed of N particles in a M-dimensional search space. Next, we can represent the velocity and position of the i-th particle can be represented as M-dimensional vectors:

$$v_i = (v_{i1}, v_{i2}, \ldots, v_{iM}), i = 1, 2, \ldots, N, \tag{18}$$

$$x_i = (x_{i1}, x_{i2}, \ldots, x_{iM}), i = 1, 2, \ldots, N, \tag{19}$$

where v_i and x_i represent the velocity vector and the position vector, respectively.

The velocity vector of particles in search space consists of three terms: the first one is the inertia or momentum component reflecting the motion habits of particles; the second one is the cognitive component that enables particles to approach their optimal position reached previously; the last one is the social component which drives particles to make their way towards

Algorithm 1: PSO Algorithm.

Input: N, M, $T_{\max}$;
Stage one
Initialize the particle position x_i and velocity v_i;
Initialize the previous local best position p_{best} and the global best position g_{best};
Stage two
While no convergence **And** iteration $\leq T_{\max}$ **do**
Update and set the velocity and position of the i-th particle according to (20) and (21);
Evaluate the fitness value using the function (16);
Update p_{best} and g_{best};
Update the iteration $t = t + 1$;
end while
Output: Optimal refractive index for RIS.

the global best position [21]. Based on the analysis, the velocity and position of the i-th particle are adjusted and updated through the following equations:

$$v_i^{(t+1)} = w v_i^{(t)} + l_1 s_1 (p_{\text{best}} - x_i^{(t)}) + l_2 s_2 (g_{\text{best}} - x_i^{(t)}), \quad (20)$$

$$x_i^{(t+1)} = x_i^{(t)} + v_i^{(t+1)}, \quad (21)$$

where t denotes the iteration of the algorithm, v_i and x_i denote the particle's velocity and position, respectively, w is the inertia weight of the movements, which is a constant value varied from 0 to 1, l_1 and l_2 are learning factors, s_1 and s_2 represent random variables between 0 and 1, p_{best} is the best local position for the i-th particle, and g_{best} represents the best position in the searching process of the entire population. In addition, $v_i \in [v_{\min}, v_{\max}]$ represents the velocity range of particles. We introduce this method to pose a minimum and maximum velocity limit to each particle, thereby preventing particles from moving too much, exceeding the search space limits.

It is worth noting that the best solutions are updated through continuous iterations. Specifically, the local solution and the global solution are updated when the calculated values are larger than the present values. At every iteration, the position and velocity of each particle are also adjusted in a limited number of directions according to their own previous experience [22]. Then, it achieves the evolution of the entire population toward the optimal direction. Finally, the iteration process ends when the maximum number of iterations is achieved or the fitness function is satisfied.

C. Complexity Analysis

The computational complexity of the PSO algorithm can be described as follows. The task of generating the initial particle population has a complexity of $O(NM)$. The initial velocity generation process involves identical operations. Selecting the best local solution and the optimal global solution found by the whole group requires $O(NM)$ operations. Thus, the above process leads to a computational complexity of $O(NM)$ at the initial stage of Algorithm 1. The worst-case for updating the position and velocity solutions has a computational complexity of $O(NMT_{\max})$, where $T_{\max}$ denotes the total number of iterations. Calculating the local best solution and choosing the global best solution for the whole population in the worst case requires operations of $O(NT_{\max})$ and $O(NT_{\max})$, respectively. Finally, the second stage of the PSO algorithm takes operations about $O(NMT_{\max})$. Therefore, the worst-case complexity of the PSO algorithm is $O(NM) + O(NMT_{\max}) \approx O(NMT_{\max})$.

TABLE I
SIMULATION PARAMETERS

Parameter	Value	Parameter	Value
$\Phi_{1/2}$	70°	η_e	1.7
A_{PD}	1 cm^2	η_a	1.0
R_{PD}	0.53 A/W	d	0.80 mm
N_o	10^{-21} A^2/Hz	q	3
B	200 MHZ	f	1.5
r_{eff}	12 pm/V	Θ_{FoV}	80°
η_o	1.5	ρ_{wall}	0.8
v_0	0.8 V	v_{th}	1.2 V
η_b	1.5	η_t	1.7
N_u	10000	λ	$\{510nm, 670nm\}$

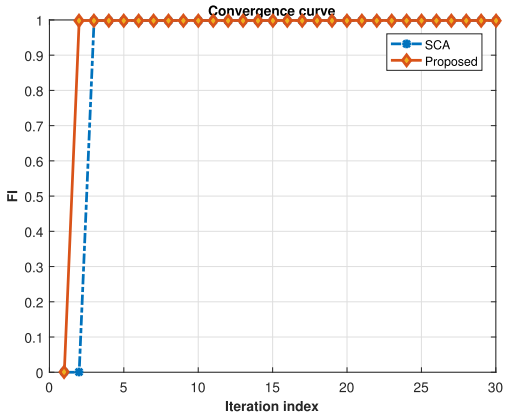

Fig. 2. The convergence rate of the PSO algorithm. At $\lambda = 510$ nm and P = 2 W.

IV. Simulation Results

This section presents the simulation results that assess the improvement in communication performance achieved by applying the LC RIS-assisted transmitter. The room dimensions are 5 m $\times$ 5 m $\times$ 3 m, and a transmitter is positioned at the center of the ceiling. The receiving plane is parallel to the floor and located at a height of 0.85 meters above the ground. To evaluate the fairness of user communication, we divide the receiving plane into 100 $\times$ 100, grids [6]. Each user in the grids is assumed to have a PD that is positioned towards the ceiling and has a normal vector that is perpendicular to the ground. We consider the four walls, each wall plane divided into 25 $\times$ 15 finite area units with identical reflectivity. The other parameters used are provided in Table I.

Fig. 2 shows the convergence of the PSO algorithm. The "SCA" represents the result achieved by the sine-cosine algorithm (SCA) and the "proposed" represents the RIS optimized by the PSO method. Obviously, the PSO algorithm converges

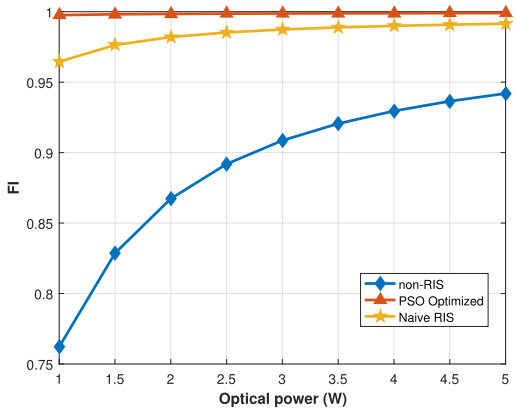

Fig. 3. The FI versus optical power for different methods in the VLC system. At $\lambda = 510$ nm.

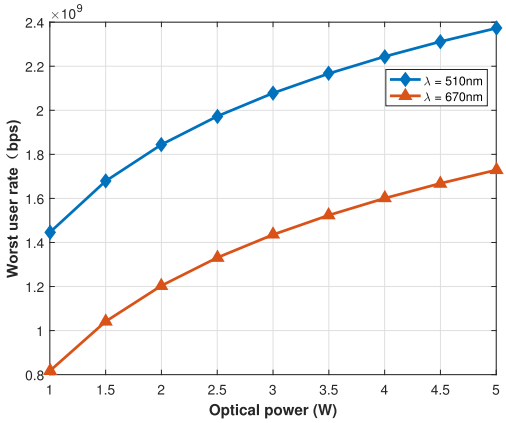

Fig. 5. The worst user rate versus different wavelengths of light signals.

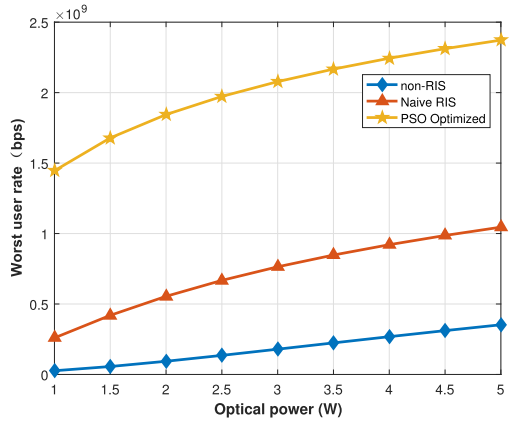

Fig. 4. The worst user rate versus transmit optical power. At $\lambda = 510$ nm.

to the solution obtained by the SCA algorithm after only a few iterations.

Fig. 3 compares the user fairness of the RIS-enabled system and its counterpart of the system without RIS. Here, "non-RIS" refers to the absence of RIS in the transmitter. The "naive RIS" indicates that the refractive index of RIS is chosen randomly [14], and the "PSO optimized" represents the refractive index optimized by Algorithm 1. Notably, when the transmission power is increased from 1 W to 5 W for the VLC system with the RIS-enabled transmitter, the user fairness index shows a steadily growing trend, and the fairness index consistently approaches a value of 1 for the proposed method. Since the refractive index obtained by the proposed method is the solution based on the fairness maximization problem we set, it outperforms the randomly selected method regarding user fairness performance. In addition, the fairness index of the proposed system is greater than that of the system without the RIS-assisted transmitter. The reason is that the LC RIS, located at the front end of the transmitter, can amplify light to different extents for users at any position on the receiving plane. As a result, deploying the LC RIS in the transmitter can significantly enhance fairness for users and minimize variations in different user communication performance compared to the system without RIS.

Fig. 4 depicts the achievable data rate of the poorest user for different transmission power values. Several interesting phenomena can be revealed from this figure. Firstly, the data rate that the weakest user can achieve increases as the transmission power increases. The observation can be explained by considering the data rate equation as a logarithmic function in (15). Secondly, the suggested optimized RIS scheme outperforms the non-RIS method, revealing that implementing RIS at the transmitting end can improve the rate of the poorest user. The enhancement of this communication performance shows the capabilities of RIS-enabled transmitters in terms of beam focusing and light amplification. Furthermore, our method can provide Gbps download speeds for the worst user at $P = 1$ W, ensuring high-quality communication. In contrast, the "naive RIS" method can only achieve a Mbps data rate for the poorest user. The effectiveness of the proposed algorithm can be demonstrated by comparing these two approaches. The above analyses reveal that the proposed system makes it possible for the worst user to obtain higher-quality communication easily.

Fig. 5 compares the rate performance of the weakest user in the RIS-aided VLC system for different optical wavelengths. The proposed scheme achieves up to 53% improvement in rate when the incident light wavelength decreases from 670 nm to 510 nm. This happens because changing the wavelength will reduce the amplification gain coefficient, thus affecting communication performance.

Fig. 6 illustrates the variations in sum rate performance for the RIS-assisted system compared with the system without RIS. This figure exhibits several interesting results. Although our objective is to enhance fairness, we observe that the sum rate is enhanced. More specifically, the integration of RIS has resulted in a 233% increase in the sum rate. The reason is that the RIS module's light amplification capability enables users on the receiving plane to receive enhanced light. Moreover, it is worth mentioning that the sum rate from LoS links is almost 14 times greater than that from NLoS links when the system does not employ RIS-assisted transmitters at $P = 2$ W. However, conditions are altered when considering the suggested transmitter. Here, the sum rate of the LoS paths is merely 1.5 times greater than that of the non-LoS paths. In addition, compared to the system that does

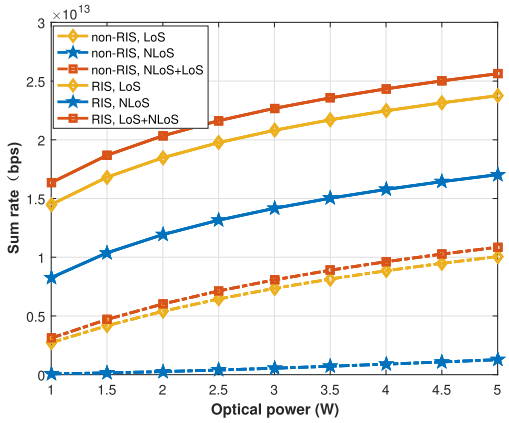

Fig. 6. The sum rate performance improvement versus optical power for directed and non-directed paths. At $\lambda = 510$ nm.

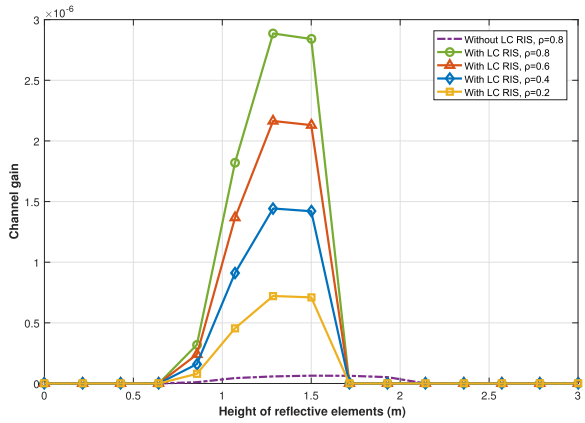

Fig. 7. NLoS channel gain resulting from the wall parallel with the $y-z$ plane versus the height of reflective elements for different wall reflectivity values.

not utilize RIS, the proposed approach enhances the sum rate for LoS and non-LoS paths by 241% and 3200%, respectively. The reason for this is that each of the interesting sub-sections for the wall can receive amplified emitted light and reflect it to the receiver at a different angle of irradiance, which is various, thus affecting the channel gain. The explanation behind this change can be attributed to the LED's Lambertian radiation model and the LC RIS's operational principles. The analysis above suggests that RIS-enabled transmitters can simultaneously enhance the performance of LoS and non-LoS paths.

Fig. 7 illustrates the channel gain variation for different heights of wall sub-regions. Since the basic principle of improving channel gains, from, NLoS, paths is similar for all users at the receiving plane, we present a representative example in this figure. We divided the wall plane into a grid of 15 rows and 25 columns. Specifically, each symbol in the figure corresponds to the non-directed channel gain from the 25 reflection units in each row of the plane parallel with the $y-z$ wall plane. We can deduce three observations from the simulation result for the system with LC-based RIS. Firstly, the channel gain is 0, with the height ranging from 0 m to 0.8 m, since the reflective area units at the top of the wall cannot receive light from the LC RIS. The reason is that LED's FoV decides which unit can receive and reflect the light signal emitted by the LC RIS. If the irradiance angle exceeds the FoV of the LED, the cosine of the irradiance angle from the transmitter towards the reflective element is 0. Secondly, we can see that the reflective unit located at the middle height of the wall is more likely to play a role in reflecting signals to the receiver. As the height of the wall reflectors ranges from 0.8 m to 1.8 m, the channel gain obtained from reflective units for each row of the wall increases and then decreases to zero. Such a trend can be explained by the Lambertian model and the functionality of LC RIS. NLoS paths rely upon reflected lights from the diffusely reflecting surface, and the reflective elements of the wall behave as receiving elements, obtaining the amplification of transmit power from LC RIS. In addition, the incidence angle at the top layer of the RIS is crucial for determining the amplification gain and transmission coefficient. Thirdly, the geometric position of the wall reflecting units at the bottom limits the reception of the reflected light, so the cosine of the incident angle is 0. This is because the PD has a limited FoV and can only detect the optical signal when the angle of incidence falls inside the FoV, according to the Lambertian model.

Fig. 7 also shows the effect of the wall reflection coefficient ρ. It is observed that the channel gain from NLoS links is reduced as ρ is changed from 0.8 to 0.2 for a given value of the height of the reflective grids. The reason is that reflection losses are very high at lower reflectivity values. Further, the result without an LC RIS-assisted transmitter is the lower bound in this figure. For a given value of ρ, the available dimension of reflecting grids that can receive the light signal using an ordinary transmitter is larger than that of the RIS-aided transmitter. Note that the amount of reflected light increases while the refracted light decreases markedly when the angle of incidence impinges on the surface of the LC module exceeds 60°. Therefore, we only consider the case where the angle of incidence does not exceed 60° for the VLC system assisted by LC RIS.

V. Conclusion

In this paper, we have proposed a refractive index of the LC-based RIS design for an indoor VLC system with the RIS-aided transmitter. In this design, a fairness maximization problem is formulated, and an intelligent PSO algorithm is employed to solve it. Simulation results have revealed that deploying RIS at the transmitter end and optimizing it via the proposed algorithm effectively improves user fairness. Hence, it is possible to improve communication performance flexibly for users on the receiving plane by placing the LC RIS at the front of the transmitters in VLC systems.

References

[1] C. Zou, F. Yang, S. Sun, Y.-J. A. Zhang, J. Song, and Z. Han, "Autoencoder for optical intelligent reflecting surface-assisted VLC system: From model and data-driven perspectives," *IEEE Internet Things J.*, vol. 10, no. 24, pp. 22487–22500, Dec. 2023.

[2] M. Seminara, T. Nawaz, S. Caputo, L. Mucchi, and J. Catani, "Characterization of field of view in visible light communication systems for intelligent transportation systems," *IEEE Photon. J.*, vol. 12, no. 4, Aug. 2020, Art. no. 7903816.

[3] S. Aboagye, A. R. Ndjiongue, T. M. N. Ngatched, and O. A. Dobre, "Design and optimization of liquid crystal RIS-based visible light communication receivers," *IEEE Photon. J.*, vol. 14, no. 6, Dec. 2022, Art. no. 7355607.

[4] S. Aboagye, T. M. N. Ngatched, O. A. Dobre, and A. R. Ndjiongue, "Intelligent reflecting surface-aided indoor visible light communication systems," *IEEE Commun. Lett.*, vol. 25, no. 12, pp. 3913–3917, Dec. 2021.

[5] S. Aboagye, A. R. Ndjiongue, T. M. N. Ngatched, O. A. Dobre, and H. V. Poor, "RIS-assisted visible light communication systems: A tutorial," *IEEE Commun. Surv. Tuts.*, vol. 25, no. 1, pp. 251–288, Firstquarter 2023.

[6] S. Aboagye, T. M. N. Ngatched, A. R. Ndjiongue, O. A. Dobre, and H. Shin, "Liquid crystal-based RIS for VLC transmitters: Performance analysis, challenges, and opportunities," *IEEE Wireless Commun.*, early access, Nov. 20, 2023, doi: 10.1109/MWC.002.2300041.

[7] F. N. Igboamalu, A. R. Ndjiongue, and K. Ouahada, "Capacity analysis of an MISO free-space optical communications assisted by concave ORIS," *J. Commun. Inf. Netw.*, vol. 8, no. 3, pp. 295–302, 2023.

[8] S. Sun, F. Yang, and J. Song, "Sum rate maximization for intelligent reflecting surface-aided visible light communications," *IEEE Commun. Lett.*, vol. 25, no. 11, pp. 3619–3623, Nov. 2021.

[9] A. R. Ndjiongue, T. M. N. Ngatched, O. A. Dobre, and H. Haas, "Reconfigurable intelligent surface-based VLC receivers using tunable liquid-crystals: The concept," *J. Lightw. Technol.*, vol. 39, no. 10, pp. 3193–3200, May 2021.

[10] O. Maraqa and T. M. N. Ngatched, "Optimized design of joint mirror array and liquid crystal-based RIS-aided VLC systems," *IEEE Photon. J.*, vol. 15, no. 4, Aug. 2023, Art. no. 7303211.

[11] O. Maraqa, S. Aboagye, and T. M. N. Ngatched, "Optical STAR-RIS-aided VLC systems: RSMA versus NOMA," *IEEE Open J. Commun. Soc.*, vol. 5, pp. 430–441, 2024.

[12] S. Abdeljabar, M. W. Eltokhey, and M.-S. Alouini, "Sum rate and fairness optimization in RIS-assisted VLC systems," *IEEE Open J. Commun. Soc.*, vol. 5, pp. 2555–2566, 2024.

[13] R. K. Jain et al., "A quantitative measure of fairness and discrimination," *Eastern Res. Laboratory, Digit. Equip. Corporation*, vol. 21, p. 1, 1984.

[14] J. Woo, C. Song, and I. Lee, "Sum rate and fairness optimization for intelligent reflecting surface aided multiuser systems," *IEEE Trans. Veh. Technol.*, vol. 70, no. 12, pp. 13436–13440, Dec. 2021.

[15] M. Hébert, R. D. Hersch, and P. Emmel, "Fundamentals of optics and radiometry for color reproduction," in *Handbook of Digital Imaging*. Hoboken, NJ, USA: John Wiley & Sons, 2015, pp. 1–57.

[16] A. R. Ndjiongue, T. M. N. Ngatched, O. A. Dobre, and H. Haas, "Digital RIS (DRIS): The future of digital beam management in RIS-assisted OWC systems," *J. Lightw. Technol.*, vol. 40, no. 16, pp. 5597–5604, Aug. 2022.

[17] V. Marinova, S. Huei Lin, R. Chung Liu, and K. Y. Hsu, "Photorefractive effect: Principles, materials, and near-infrared holography," *Wiley Encyclopedia Elect. Electron. Eng.*, pp. 1–20, 1999.

[18] A. Singh, A. Srivastava, and V. A. Bohara, "Optimum led semiangle and the receiver FOV selection for indoor VLC system with human blockages," in *Proc. IEEE 95th Veh. Technol. Conf., (VTC2022-Spring)*, 2022, pp. 1–7.

[19] T. Komine and M. Nakagawa, "Fundamental analysis for visible-light communication system using led lights," *IEEE Trans. Consum. Electron.*, vol. 50, no. 1, pp. 100–107, Feb. 2004.

[20] J. Li, C.-H. Wen, S. Gauza, R. Lu, and S.-T. Wu, "Refractive indices of liquid crystals for display applications," *J. Display Technol.*, vol. 1, no. 1, pp. 51–61, 2005.

[21] F. Marini and B. Walczak, "Particle swarm optimization (PSO). A tutorial," *Chemometrics Intell. Lab. Syst.*, vol. 149, pp. 153–165, 2015.

[22] Y. Shi and R. Eberhart, "Empirical study of particle swarm optimization," in *Proc. IEEE Congr. Evol. Computation-CEC99 (Cat. No 99TH8406)*, 1999, vol. 3, pp. 1945–1950.